

# POPULATION PARAMETERS OF INTERMEDIATE-AGE STAR CLUSTERS IN THE LARGE MAGELLANIC CLOUD. III. DYNAMICAL EVIDENCE FOR A RANGE OF AGES BEING RESPONSIBLE FOR EXTENDED MAIN-SEQUENCE TURNOFFS\*

PAUL GOUDFROOIJ<sup>1</sup>, THOMAS H. PUZIA<sup>2</sup>, RUPALI CHANDAR<sup>3</sup>, AND VERA KOZHURINA-PLATAIS<sup>1</sup>

<sup>1</sup> Space Telescope Science Institute, 3700 San Martin Drive, Baltimore, MD 21218, USA; [goudfroo@stsci.edu](mailto:goudfroo@stsci.edu), [verap@stsci.edu](mailto:verap@stsci.edu)

<sup>2</sup> Department of Astronomy and Astrophysics, Pontificia Universidad Católica de Chile, Av. Vicuña Mackenna 4860, Macul 7820436, Santiago, Chile; [tpuzia@gmail.com](mailto:tpuzia@gmail.com)

<sup>3</sup> Department of Physics and Astronomy, The University of Toledo, 2801 West Bancroft Street, Toledo, OH 43606, USA; [rupali.chandar@utoledo.edu](mailto:rupali.chandar@utoledo.edu)

Received 2011 March 29; accepted 2011 May 13; published 2011 July 20

## ABSTRACT

We present a new analysis of 11 intermediate-age (1–2 Gyr) star clusters in the Large Magellanic Cloud based on *Hubble Space Telescope* imaging data. Seven of the clusters feature main-sequence turnoff (MSTO) regions that are wider than can be accounted for by a simple stellar population, whereas their red giant branches (RGBs) indicate a single value of [Fe/H]. The star clusters cover a range in present-day mass from about  $1 \times 10^4 M_{\odot}$  to  $2 \times 10^5 M_{\odot}$ . We compare radial distributions of stars in the upper and lower parts of the MSTO region, and calculate cluster masses and escape velocities from the present time back to a cluster age of 10 Myr. Our main result is that for all clusters in our sample with estimated escape velocities  $v_{\text{esc}} \gtrsim 15 \text{ km s}^{-1}$  at an age of 10 Myr, the stars in the brightest half of the MSTO region are significantly more centrally concentrated than the stars in the faintest half *and* more massive RGB and asymptotic giant branch stars. This is not the case for clusters with  $v_{\text{esc}} \lesssim 10 \text{ km s}^{-1}$  at an age of 10 Myr. We argue that the wide MSTO region of such clusters is caused mainly by a  $\sim 200$ – $500$  Myr range in the ages of cluster stars due to extended star formation within the cluster from material shed by first-generation stars featuring slow stellar winds. Dilution of this enriched material by accretion of ambient interstellar matter is deemed plausible if the spread of [Fe/H] in this ambient gas was very small when the second-generation stars were formed in the cluster.

*Key words:* globular clusters: general – Magellanic Clouds

*Online-only material:* color figures

## 1. INTRODUCTION

For several decades, the standard paradigm for globular clusters (GCs) was that they consist of stars born at the same time out of the same material. This scenario has faced serious challenges over the last decade. It is now known that the most massive GCs in our Galaxy such as  $\omega$  Cen and M 54 host multiple red giant branches (RGBs) due to populations with different [Fe/H] (e.g., Sarajedini & Layden 1995; Lee et al. 1999; Hilker & Richtler 2000; Villanova et al. 2007; Carretta et al. 2010). Somewhat less massive Galactic GCs such as NGC 2808, NGC 1851, and 47 Tuc show multiple sub-giant branches and/or multiple main sequences (MSs), which are typically interpreted as populations with different helium abundances (e.g., Piotto et al. 2007; Milone et al. 2008; Anderson et al. 2009). While lower-mass Galactic GCs typically do not show clear evidence for multiple populations from optical broadband photometry, spectroscopic surveys do show that light elements such as C, N, O, F, and Na show significant star-to-star abundance variations (often dubbed “Na–O anticorrelations”) within all Galactic GCs studied to date in sufficient detail (Carretta et al. 2009, and references therein). Since these abundance variations have been found among RGB stars as well as MS stars within a given GC (Gratton et al. 2004), the suggested cause of the variations is that secondary generation(s) of stars formed out of material shed by an older, evolved population

within the cluster. While the chemical processes responsible for causing the light element abundance variations have largely been identified as proton-capture reactions in hydrogen burning at high temperature ( $\gtrsim 40 \times 10^6$  K; see, e.g., Gratton et al. 2004), the old age of Galactic GCs has precluded a clear picture of the timescales and hence the types of stars involved in the chemical enrichment of the second-generation stars. Currently, the most popular candidates are (1) intermediate-mass asymptotic giant branch (AGB) stars ( $4 \lesssim M/M_{\odot} \lesssim 8$ , hereafter IM-AGB; e.g., D’Antona & Ventura 2007, and references therein), (2) rapidly rotating massive stars (often referred to as “FRMS;” e.g., Decressin et al. 2007), and (3) massive binary stars (de Mink et al. 2009).

Recently, deep color–magnitude diagrams (CMDs) from images taken with the Advanced Camera for Surveys (ACS) on board the *Hubble Space Telescope* (HST) provided conclusive evidence that several massive intermediate-age star clusters in the Magellanic Clouds host extended and/or multiple main-sequence turn-off (MSTO) regions (Mackey et al. 2008; Glatt et al. 2008; Milone et al. 2009; Goudfrooij et al. 2009, hereafter Paper I; Goudfrooij et al. 2011, hereafter Paper II), in some cases accompanied by composite red clumps (RCs; Girardi et al. 2009; Rubele et al. 2011). To date, these observed properties have been interpreted in three main ways: (1) bimodal age distributions (Mackey et al. 2008; Milone et al. 2009), (2) age spreads of 200–500 Myr (Paper II; Girardi et al. 2009; Rubele et al. 2010, 2011), and (3) spreads in rotation velocity among turnoff stars (Bastian & de Mink 2009).

In this third paper of this series, we study the dynamical properties of 11 intermediate-age star clusters in the Large

\* Based on observations with the NASA/ESA *Hubble Space Telescope*, obtained at the Space Telescope Science Institute, which is operated by the Association of Universities for Research in Astronomy, Inc., under NASA contract NAS5-26555.

**Table 1**  
Main Properties of the eMSTO Star Clusters Studied in This Paper

Cluster (1)	$V$ (2)	Reference (3)	SWB (4)	Age (5)	$[Z/H]$ (6)	$A_V$ (7)
NGC 1751	$11.67 \pm 0.13$	1	VI	$1.40 \pm 0.10$	$-0.3 \pm 0.1$	$0.40 \pm 0.01$
NGC 1783	$10.39 \pm 0.03$	1	V	$1.70 \pm 0.10$	$-0.3 \pm 0.1$	$0.02 \pm 0.02$
NGC 1806	$11.00 \pm 0.05$	1	V	$1.67 \pm 0.10$	$-0.3 \pm 0.1$	$0.05 \pm 0.01$
NGC 1846	$10.68 \pm 0.20$	1	VI	$1.75 \pm 0.10$	$-0.3 \pm 0.1$	$0.08 \pm 0.01$
NGC 1987	$11.74 \pm 0.09$	1	IVB	$1.05 \pm 0.05$	$-0.3 \pm 0.1$	$0.16 \pm 0.04$
NGC 2108	$12.32 \pm 0.04$	2 <sup>a</sup>	IVB	$1.00 \pm 0.05$	$-0.3 \pm 0.1$	$0.50 \pm 0.03$
LW 431	$13.67 \pm 0.04$	2 <sup>a</sup>	VI	$1.75 \pm 0.10$	$-0.3 \pm 0.1$	$0.15 \pm 0.01$

**Notes.** Column 1: name of star cluster. Column 2: integrated  $V$  magnitude. Column 3: reference of  $V$  magnitude. Reference 1: Goudfrooij et al. (2006); reference 2: Bica et al. (1996). Column 4: SWB type from Bica et al. (1996). Column 5: age in Gyr from Paper II. Column 6: metallicity from Paper II. Column 7:  $A_V$  from Paper II.

<sup>a</sup> Uncertainty only includes internal errors associated with measurements of cluster and one background aperture.

Magellanic Cloud (LMC): seven clusters that exhibit extended MSTO regions (hereafter eMSTOs) and four that do not. We determine and compare radial distributions of cluster stars at different evolutionary phases and evaluate the evolution of the clusters' masses and escape velocities from an age of 10 Myr to their current age. This analysis reveals new findings relevant to the assembly of these intermediate-age star clusters and their evolutionary association with multiple stellar populations in ancient Galactic GCs.

The remainder of this paper is organized as follows. Section 2 presents the cluster sample. In Section 3, we determine the radial distributions of stars in various different evolutionary phases and study the dependencies of these distributions with cluster escape velocities as a function of time. Section 4 uses our new results to constrain the origin of multiple populations in these clusters, and Section 5 presents our main conclusions.

## 2. TARGET CLUSTERS

Our main sample of intermediate-age clusters is that presented in Paper II. All these clusters were observed within one *HST*/ACS program using the same observational setup, using both short and long exposures to yield high-quality photometry throughout the CMDs. The sample consists of star clusters in the LMC with integrated  $UBV$  colors consistent with SWB (Searle et al. 1980) parameter values in the range IV B–VI, which translates to estimated ages between roughly 1.0 and 2.5 Gyr. This turned out to be fully consistent with the ages actually found from isochrone fitting. The main properties of these star clusters, all of which were found to host eMSTO regions, are listed in Table 1. For comparison with clusters in the same age range that do *not* contain eMSTO regions, we also use the four LMC clusters NGC 1644, NGC 1652, NGC 1795, and IC 2146 that were studied by Milone et al. (2009) using *HST*/ACS photometry. To our knowledge, these are the only four clusters in the LMC in the age range 1–2 Gyr that are known to date *not* to harbor eMSTO regions (Milone et al. 2009) from high-quality photometry at *HST* resolution.

## 3. RADIAL DISTRIBUTIONS OF STARS IN DIFFERENT REGIONS OF THE CMD

### 3.1. Motivation

Since the eMSTO regions in our target clusters may be due to the presence of more than one simple stellar population, it is important to find out whether different subregions of the eMSTO

have intrinsically different radial distributions, i.e., differences beyond those that can be expected for simple (coeval) stellar populations due to dynamical evolution. A well-known example of the latter is mass segregation due to dynamical friction which slows down stars on a timescale that is inversely proportional to the mass of the star (e.g., Saslaw 1985; Spitzer 1987; Meylan & Heggie 1997) so that massive stars have a more centrally concentrated distribution over time than less massive ones. Another reason for studying the radial distributions of stars in relevant evolutionary phases in the CMD is that the masses and ages of these clusters are such that the two-body relaxation times of stars within the clusters are comparable to the cluster ages: the mean two-body relaxation time  $t_{\text{relax}}$  of stars within a cluster's half-mass radius is

$$t_{\text{relax}} \approx \frac{N}{8 \ln N} t_{\text{cross}} \approx \frac{N}{8 \ln N} r_h^{1.5} (G \mathcal{M}_{\text{cl}})^{-0.5} \quad (1)$$

(Binney & Tremaine 1987), where  $t_{\text{cross}}$  is the crossing time at the half-mass radius,  $N$  is the number of stars in the cluster,  $r_h$  is the half-mass radius,  $G$  is the gravitational constant, and  $\mathcal{M}_{\text{cl}}$  is the cluster mass.  $t_{\text{relax}}$  values for the clusters in our sample are listed in Table 2. For a typical cluster among the 50% most massive clusters in our sample,  $N \simeq 1.5 \times 10^5$ ,  $\mathcal{M}_{\text{cl}} \simeq 10^5 M_{\odot}$ , and  $r_h \simeq 8$  pc, resulting in  $t_{\text{relax}} \simeq 2$  Gyr. Hence, dynamical imprints from the formation epoch of the stars within these clusters may well be still observable, in contrast to the situation in the vast majority of Galactic GCs ( $\omega$  Cen is the exception; see, e.g., Bellini et al. 2009). This renders these intermediate-age clusters excellent probes of the nature of multiple stellar populations in star clusters.

### 3.2. Measurements and Implications

We derived radial distributions of the following regions on the CMDs of the seven star clusters in our sample that contain eMSTOs: (1) “all” stars in the CMD, (2) the “upper half” of the eMSTO region, (3) the “lower half” of the eMSTO region, and (4) the RC stars and the RGB and AGB stars above the RC. Note that regions (2)–(4) were found in Paper II to have less than 5% contamination by field stars for every cluster. Figure 1 depicts these regions on the CMD of NGC 1806 with solid lines, while the completeness-corrected radial distributions of stars in these regions are shown in Figure 2. The size of radial bins in all panels of Figure 2 was determined by the requirement that there be at least 30 stars in the outermost radial bin for any of the CMD regions considered.

**Table 2**  
Adopted Dynamical Parameters of the eMSTO Star Clusters Studied in This Paper

Cluster (1)	$\log(\mathcal{M}_{cl}/M_{\odot})$		$r_h$		$t_{relax}$		$v_{esc}$		$C_{rel}$ (10)
	Current (2)	$10^7$ yr (3)	Current (4)	$10^7$ yr (5)	Current (6)	$10^7$ yr (7)	Current (8)	$10^7$ yr (9)	
Case I: model without initial mass segregation									
NGC 1751	$4.82 \pm 0.09$	$5.07 \pm 0.09$	$7.1 \pm 0.6$	$5.0 \pm 0.4$	$1.2 \pm 0.2$	$0.9 \pm 0.1$	$9.2 \pm 0.9$	$14.6 \pm 1.5$	$2.52 \pm 0.53$
NGC 1783	$5.25 \pm 0.09$	$5.46 \pm 0.09$	$14.7 \pm 3.2$	$9.9 \pm 2.2$	$5.2 \pm 1.8$	$3.8 \pm 1.3$	$9.9 \pm 1.5$	$12.6 \pm 2.3$	$1.33 \pm 0.07$
NGC 1806	$5.03 \pm 0.09$	$5.27 \pm 0.09$	$8.9 \pm 0.6$	$6.3 \pm 0.4$	$2.0 \pm 0.2$	$1.5 \pm 0.2$	$10.3 \pm 1.2$	$16.3 \pm 1.6$	$2.06 \pm 0.16$
NGC 1846	$5.17 \pm 0.09$	$5.41 \pm 0.09$	$8.4 \pm 0.4$	$5.9 \pm 0.3$	$2.1 \pm 0.2$	$1.5 \pm 0.1$	$12.7 \pm 1.2$	$20.0 \pm 1.9$	$3.36 \pm 0.18$
NGC 1987	$4.49 \pm 0.09$	$4.73 \pm 0.09$	$8.9 \pm 2.2$	$6.2 \pm 1.5$	$1.2 \pm 0.4$	$0.9 \pm 0.3$	$5.6 \pm 0.8$	$8.8 \pm 1.3$	$1.55 \pm 0.37$
NGC 2108	$4.41 \pm 0.09$	$4.66 \pm 0.09$	$7.1 \pm 0.6$	$5.0 \pm 0.4$	$0.8 \pm 0.1$	$0.6 \pm 0.1$	$5.7 \pm 0.6$	$9.1 \pm 0.9$	$1.45 \pm 0.62$
LW 431	$4.00 \pm 0.09$	$4.31 \pm 0.09$	$7.2 \pm 1.7$	$5.1 \pm 1.2$	$0.6 \pm 0.2$	$0.4 \pm 0.2$	$3.5 \pm 0.5$	$6.0 \pm 0.9$	$1.27 \pm 0.61$
Case II: model involving initial mass segregation									
NGC 1751	$4.82 \pm 0.09$	$5.17 \pm 0.09$	$7.1 \pm 0.6$	$2.6 \pm 0.2$	$1.2 \pm 0.2$	$0.4 \pm 0.1$	$9.2 \pm 0.9$	$22.6 \pm 2.3$	$2.52 \pm 0.53$
NGC 1783	$5.25 \pm 0.09$	$5.58 \pm 0.09$	$14.7 \pm 3.2$	$5.5 \pm 1.1$	$5.2 \pm 1.8$	$1.6 \pm 0.6$	$9.9 \pm 1.5$	$20.2 \pm 3.0$	$1.33 \pm 0.07$
NGC 1806	$5.03 \pm 0.09$	$5.37 \pm 0.09$	$8.9 \pm 0.6$	$3.3 \pm 0.2$	$2.0 \pm 0.3$	$0.6 \pm 0.1$	$10.3 \pm 1.2$	$25.3 \pm 2.5$	$2.06 \pm 0.16$
NGC 1846	$5.17 \pm 0.09$	$5.52 \pm 0.09$	$8.4 \pm 0.4$	$3.1 \pm 0.1$	$2.1 \pm 0.3$	$0.7 \pm 0.1$	$12.7 \pm 1.2$	$31.0 \pm 3.0$	$3.36 \pm 0.18$
NGC 1987	$4.49 \pm 0.09$	$4.82 \pm 0.09$	$8.9 \pm 2.2$	$3.3 \pm 0.8$	$1.2 \pm 0.5$	$0.4 \pm 0.1$	$5.6 \pm 0.8$	$13.5 \pm 2.0$	$1.55 \pm 0.37$
NGC 2108	$4.41 \pm 0.09$	$4.75 \pm 0.09$	$7.1 \pm 0.6$	$2.7 \pm 0.2$	$0.8 \pm 0.1$	$0.3 \pm 0.1$	$5.7 \pm 0.6$	$13.5 \pm 2.0$	$1.45 \pm 0.62$
LW 431	$4.00 \pm 0.09$	$4.41 \pm 0.09$	$7.2 \pm 1.7$	$2.7 \pm 0.6$	$0.6 \pm 0.2$	$0.2 \pm 0.1$	$3.5 \pm 0.5$	$9.3 \pm 1.3$	$1.27 \pm 0.61$

**Notes.** Column 1: name of star cluster. Column 2: logarithm of adopted current cluster mass (in solar masses). Column 3: logarithm of adopted cluster mass at an age of 10 Myr. Column 4: current cluster half-mass radius in pc. Column 5: adopted cluster half-mass radius at an age of 10 Myr. Column 6: current cluster half-mass relaxation time in Gyr. Column 7: cluster half-mass relaxation time at an age of 10 Myr. Column 8: current cluster escape velocity at tidal radius in  $\text{km s}^{-1}$ . Column 9: cluster escape velocity at tidal radius at an age of 10 Myr. Column 10: value of  $C_{rel}$ , defined in Section 3.3.4.

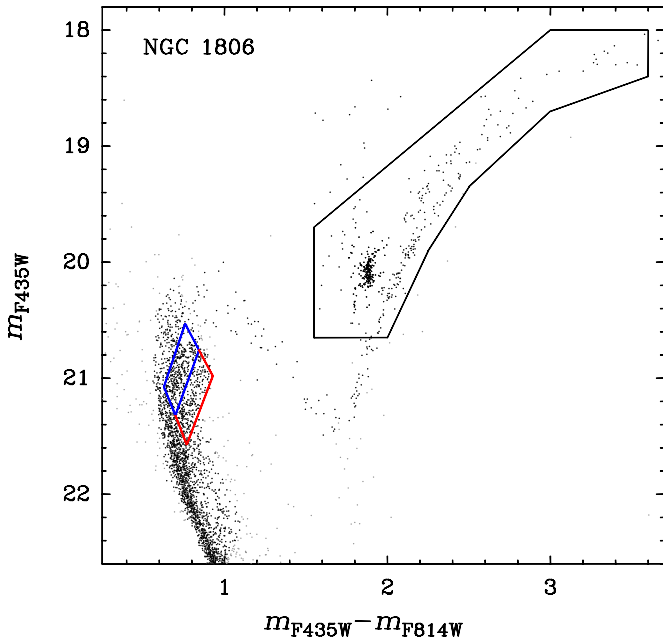


**Figure 1.** Illustration of the three regions used to derive the radial surface number density distributions shown in Figure 2, superposed onto the CMD of NGC 1806 as shown in the middle panel of Figure 2 of Paper II. The upper MSTO region is outlined by blue solid lines, the lower MSTO region by red lines, and the RC, RGB, and AGB by black lines.

Figure 2 shows several items of interest, discussed in turn below.

1. For many of the brighter (more massive) clusters in our sample, the stars in the upper (brighter) half of the eMSTO region are significantly more centrally concentrated than the stars in the lower (fainter) half of the eMSTO. In fact, the stars in the upper half of the eMSTO show a central con-

centration that is even stronger than that of (more massive) stars in the upper RGB/AGB in the clusters NGC 1751 and NGC 1846 (and, to a somewhat lesser extent, NGC 1806). This means that mass segregation cannot be the cause of these differences. The radial distribution of the RGB/AGB stars in these three massive clusters typically follows that of the lower half of the eMSTO except for the innermost few radial bins where it is intermediate between the radial distributions of the upper and lower halves of the eMSTO region.

2. Interestingly, this difference in central concentration between the upper and lower halves of the eMSTO is not quite as strong for NGC 1783, the most luminous cluster in our sample. The case of NGC 1783 is discussed in some detail in Section 3.3.4 below.
3. The difference in central concentration between the upper and lower halves of the eMSTO is insignificant for the lower-luminosity clusters LW 431, NGC 1987, and NGC 2108.
4. Finally, the radial gradient of “all” stars in the clusters (open circles in Figure 2) is significantly shallower than that of the MSTO and RGB/AGB populations. This mainly reflects the relatively strong contamination by LMC field stars in the lower MS region of the CMD of these clusters (see Paper II).

We conclude that the upper and lower parts of the eMSTOs in (at least some of) these star clusters correspond to intrinsically physically different populations which seem to have experienced different amounts of violent relaxation during their collapse and/or different dynamical evolution effects.

We believe that this finding is relevant in the context of the two main interpretations of the eMSTO regions in the recent literature: (1) bimodal age distributions or spreads in age (Mackey et al. 2008; Milone et al. 2009; Girardi et al. 2009; Paper I; Paper II) and (2) spreads in rotation velocity among

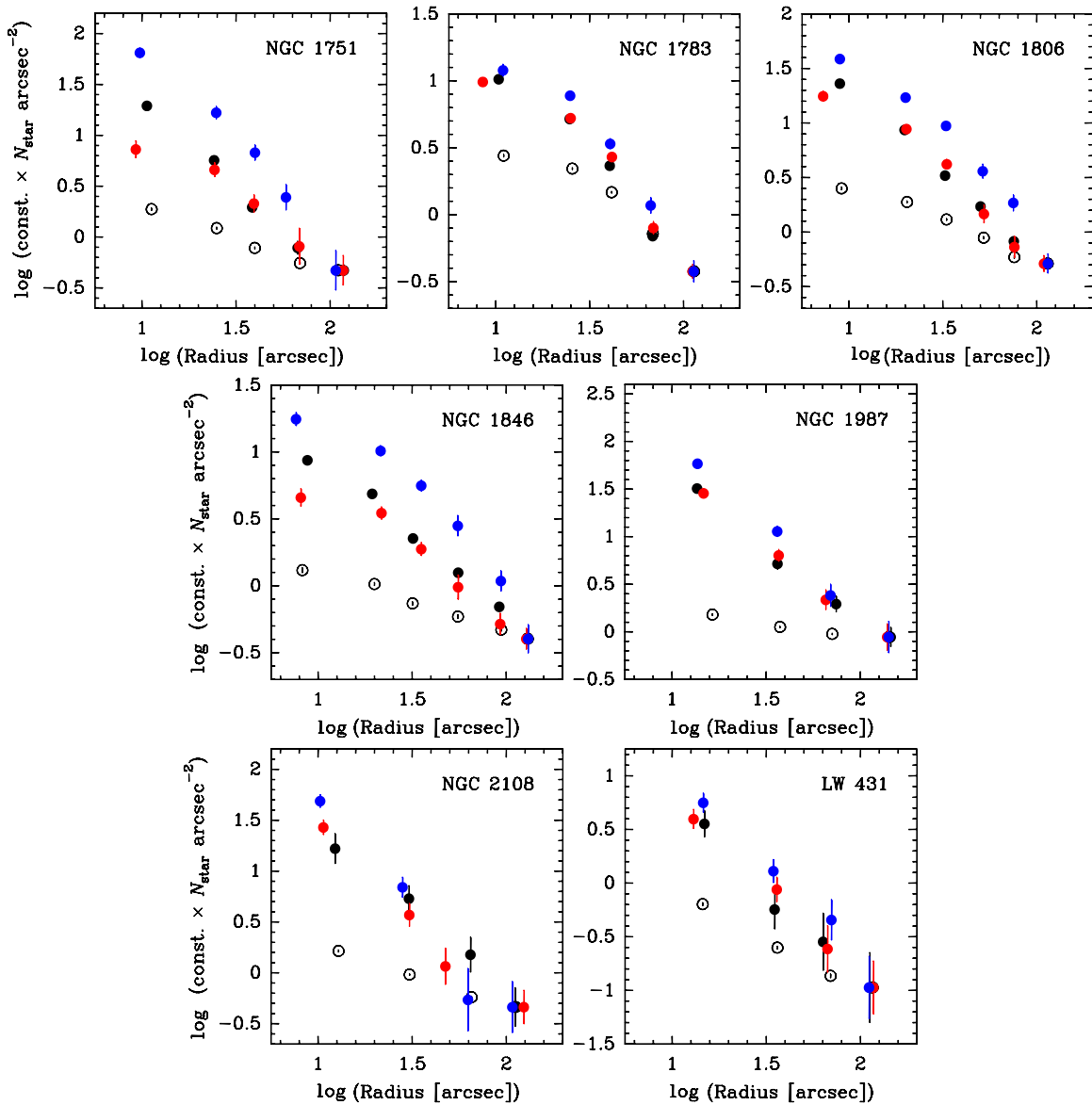


**Figure 2.** Radial surface number density distributions of stars in different evolutionary phases, as illustrated in the CMD in Figure 1 with solid lines. Cluster names are given in the top right in each panel. Open circles: all stars in the CMD. Black circles: stars in the RC, RGB, and AGB. Red circles: lower MSTO region. Blue circles: upper MSTO region. The absolute surface number density values on the Y-axis refer to the open circles (“all stars”). The surface number densities of the other star types are normalized to that of “all stars” at the outermost radial bin. See discussion in Section 3.

turnoff stars (Bastian & de Mink 2009, but see Girardi et al. 2011). Specifically, if the width of the eMSTO in intermediate-age star clusters is caused mainly by one or more secondary generation(s) of stars having formed within the cluster from material shed in slow winds of stars of the first generation and retained by the cluster, the simulations of D’Ercole et al. (2008) show that the younger generation (i.e., the *upper* half of the eMSTO region) would be more centrally concentrated than the older one if the age of the cluster is less than or similar to the half-mass relaxation time (which is the case for the four most massive clusters in our sample, cf. Table 2). Conversely, if the width of the eMSTO is due mainly to a range in rotation speeds among stars with masses  $1.2 \lesssim M/M_{\odot} \lesssim 1.7$  (Bastian & de Mink 2009), one might expect more rapid rotators (i.e., the *lower* half of the eMSTO region according to Bastian & de Mink 2009) to be initially more centrally concentrated than less rapid rotators since observational studies have found young stars in dense star clusters to show higher rotation rates than similar

stars in the field and hence born in presumably less dense stellar aggregates (e.g., Keller 2004; Strom et al. 2005). While detailed modeling of the dependencies of the radial distribution of stars in star clusters on stellar rotation velocity and cluster age is still lacking, the observation that the upper (i.e., brighter) half of the eMSTO population is significantly more centrally concentrated than the lower (i.e., fainter) half in several star clusters in our sample seems to indicate that age effects *are* responsible for the broadening of the eMSTO (at least in those clusters).

### 3.3. Trends with Cluster Escape Velocity as a Function of Time

In a scenario where secondary generations form from material shed in slow stellar winds of the first generation, expected wind speeds for intermediate-mass AGB (IM-AGB) stars are about  $10\text{--}20 \text{ km s}^{-1}$  (e.g., Vassiliadis & Wood 1993; Marshall et al. 2004). For fast-rotating massive stars (FRMS), wind speeds range between about ten to a few hundreds of  $\text{km s}^{-1}$  (Porter 1996; Porter & Rivinius 2003; Wunsch et al. 2008). For massive

interacting binary stars, one can expect wind velocities of a few tens of  $\text{km s}^{-1}$  as well: observations of the well-studied system RY Scuti have shown ejection velocities of  $30\text{--}70 \text{ km s}^{-1}$  (Smith et al. 2002; de Mink et al. 2009). If any (or all) of these types of stars provide the material for secondary generations in star clusters, one would expect the ability of star clusters to retain this material to scale with their escape velocities at the time such stars are present in the cluster (i.e., at ages of  $\sim 5\text{--}30 \text{ Myr}$  for the massive stars and  $\sim 50\text{--}200 \text{ Myr}$  for IM-AGB stars). Furthermore, a well-defined relation has been suggested to exist between the most massive star in a cluster and the initial cluster cloud mass in that initially more massive clusters host more massive stars. The physical effect that causes this relation may be that retention of feedback energy from more massive stars requires more massive gas clouds (Weidner & Kroupa 2006). Hence, if massive stars are a significant source of the material used to form secondary generations in clusters, one would expect the existence of a relation between the fraction of second-generation stars and the mass of the cluster.

With this in mind, we estimate masses and escape velocities of the clusters in our sample for both the present time and at an age of  $10^7 \text{ yr}$  (i.e., after the cluster has survived the era of gas expulsion and violent relaxation; see, e.g., Baumgardt et al. 2008) as follows. For comparison with clusters in the same age range that do *not* contain eMSTO regions, we also do these calculations for the four LMC clusters NGC 1644, NGC 1652, NGC 1795, and IC 2146 from the study of Milone et al. (2009).

### 3.3.1. Present-day Masses and Half-mass Radii

Present-day masses and half-mass radii for the clusters in our sample are adopted from Paper II (see its Tables 1 and 3), using  $M/L_V$  ratios of the SSP models of Bruzual & Charlot (2003). For the four clusters found by Milone et al. (2009) not to contain eMSTOs, we use the total  $V$ -band magnitudes in Bica et al. (1996) along with age, distance, and foreground reddening values from Milone et al. (2009). Since we cannot find half-light radii published for those four clusters in the literature, we assume an average value of clusters in the LMC within the age range  $1\text{--}2 \text{ Gyr}$  from the literature (Mackey & Gilmore 2003; Paper II) along with a suitably large uncertainty, namely  $r_h = 8 \pm 4 \text{ pc}$ .

### 3.3.2. Early Cluster Mass Loss

We make a distinction between model clusters with and without initial mass segregation, the inclusion of which can have a strong impact on cluster mass loss and dissolution due to the strong expansion of the cluster in response to rapid mass loss associated with supernova (SN) type II explosions of first-generation stars (e.g., Chernoff & Weinberg 1990; Fukushige & Heggie 1995; Vesperini et al. 2009). To properly represent the case of clusters with initial mass segregation for this paper, a selection needs to be made as to the initial properties of the cluster since the recent literature shows that different initial properties can lead to a wide range of cluster dissolution times (Baumgardt & Kroupa 2007; Baumgardt et al. 2008; D’Ercole et al. 2008; Vesperini et al. 2009). We consider the evolution of cluster mass and half-mass radius in the simulation called SG-C30 in D’Ercole et al. (2008; E. Vesperini 2011, private communication), which involves a tidally limited model cluster that features a moderate degree of initial mass segregation. This simulation is selected for the following reasons: (1) mass-segregated clusters of this type can survive the rapid SN-driven mass-loss era (Vesperini et al. 2009); (2) it yields a ratio of first-to-second-generation stars of  $\sim 1:1$  at an age of  $2 \text{ Gyr}$

(see Figure 16 of D’Ercole et al. 2008), similar to (though somewhat lower than) what has been found for the more massive clusters in our sample (see Paper II; Milone et al. 2009). Note that simulations of clusters with initially more strongly mass-segregated stellar distributions can yield results similar to that of the SG-C30 simulation if the cluster does not fully fill its Roche lobe (Vesperini et al. 2009). We also account for the effect of mass loss due to stellar evolution, most of which takes place in the first  $10^8 \text{ yr}$ . The evolution of this mass loss is derived using the Bruzual & Charlot (2003) SSP models using the Chabrier (2003) IMF.<sup>4</sup> The fast stellar evolution-driven mass loss in the first  $10^8 \text{ yr}$ , in particular that due to feedback and SNe from massive O and B-type stars, also causes an expansion of the cluster. This is accounted for by following the prescriptions of Hills (1980) assuming adiabatic expansion, since the crossing time of star clusters is much shorter than the timescale for stellar evolution-driven mass loss (see also Baumgardt et al. 2008).

### 3.3.3. Long-term Cluster Mass Loss

At ages  $> 100 \text{ Myr}$  we account for long-term dynamical cluster destruction mechanisms and follow Fall & Zhang (2001) and McLaughlin & Fall (2008) who find that the change in shape of the star cluster mass function from young ( $\lesssim 5 \times 10^8 \text{ yr}$ ) to old ( $\gtrsim 10^{10} \text{ yr}$ ) systems is due mainly to mass-density-dependent evaporation (also often called “two-body relaxation”). We use the rate of mass loss due to evaporation derived by McLaughlin & Fall (2008, their Equation (5)):

$$\overline{\mu_{\text{ev}}} \simeq 1100 \left( \frac{\rho_h}{M_\odot \text{ pc}^{-3}} \right)^{1/2} M_\odot \text{ Gyr}^{-1}, \quad (2)$$

where  $\overline{\mu_{\text{ev}}}$  is the mass-loss rate due to evaporation averaged over a cluster lifetime and  $\rho_h \equiv 3 \mathcal{M}_{\text{cl}} / 8\pi r_h^3$  is the half-mass density of the star cluster. The evolution of cluster masses is then calculated for an appropriately large grid of masses and half-mass radii at an age of  $13 \text{ Gyr}$ , both with and without initial mass segregation (implemented as described in the previous paragraph). Cluster mass as a function of time for individual star clusters in our sample is evaluated by means of linear interpolation between grid lines using masses at the mean age of the cluster in question. The process of calculating cluster masses as a function of time is illustrated in Figure 3 for the case of NGC 1846. For a typical cluster in our sample, the difference in initial cluster mass between mass-segregated and non-mass-segregated star clusters is of order  $\Delta \log \mathcal{M}_{\text{cl}} \approx 0.1\text{--}0.15 \text{ dex}$ , with the initially mass-segregated clusters losing a larger fraction of their initial mass.

### 3.3.4. Escape Velocities

Escape velocities required to reach the tidal radius of the cluster are calculated as follows:

$$v_{\text{esc}}(t) = f_c \sqrt{\frac{\mathcal{M}_{\text{cl}}(t)}{r_h(t)}} \text{ km s}^{-1}, \quad (3)$$

where  $\mathcal{M}_{\text{cl}}(t)$  is the cluster mass in  $M_\odot$  at time  $t$ ,  $r_{h,t}(t)$  is the cluster’s half-light radius in pc at time  $t$ , and  $f_c$  is a coefficient that takes the dependence of  $v_{\text{esc}}$  on the concentration index  $c$  of King (1962) models into account. Values for  $f_c$  are

<sup>4</sup> Use of the Salpeter (1955) IMF results in initial cluster masses that are  $\sim 9\%$  lower than those calculated here.

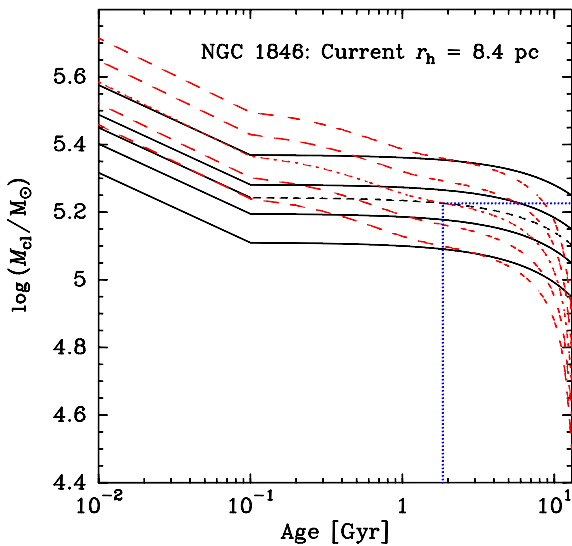


**Figure 3.** Illustration of the method used to calculate cluster masses as a function of age. (Black) solid lines and the short-dashed line represent calculations for initially non-mass-segregated clusters, whereas (red) long-dashed lines and the (red) dash-dotted line represent calculations for an initially mass-segregated cluster model (see discussion in Section 3.3). Four model calculations are shown for the current half-mass radius of NGC 1846 and spaced by  $\log(M_{cl}/M_{\odot}) = 0.1$  at an age of 13 Gyr. The short-dashed and dash-dotted lines depict the adopted mass evolution for NGC 1846. The (blue) dotted lines indicate the current age and mass of NGC 1846.

(A color version of this figure is available in the online journal.)

taken from Georgiev et al. (2009). For convenience, we define  $v_{esc,7} \equiv v_{esc}(10^7 \text{ yr})$  hereinafter.

To parameterize the relative central concentrations of the upper and lower half of the eMSTO region in the star clusters, we define a “relative concentration parameter” as follows:

$$C_{rel} \equiv \frac{(n_{core,upp} - n_{bck,upp})}{n_{bck,upp}} \bigg/ \frac{(n_{core,low} - n_{bck,low})}{n_{bck,low}}, \quad (4)$$

where  $n_{core,upp}$  and  $n_{bck,upp}$  are surface number densities of stars in the upper half of the eMSTO region within the King core radius and the background region, respectively, and  $n_{core,low}$  and  $n_{bck,low}$  are the same parameters for stars in the lower half of the eMSTO region. The background region was defined as the

outermost radial bin used for the plots in Figure 2. Values for  $M_{cl}$ ,  $r_h$ ,  $t_{relax}$ ,  $v_{esc}$ , and  $C_{rel}$  are given in Table 2, both for the present time and at an age of  $10^7$  yr. We adopt an uncertainty of 20% for present-day cluster mass values and use that in calculating the uncertainties in  $t_{relax}$  and  $v_{esc}$ .

$C_{rel}$  is plotted versus cluster  $v_{esc}$  at the current age and at an age of  $10^7$  yr in the two panels of Figure 4. By definition, we set  $C_{rel} \equiv 1$  for the clusters found by Milone et al. (2009) not to host eMSTOs. The left panel shows that the clusters with the highest current escape velocities tend to have the highest value of  $C_{rel}$ , although the current escape velocities are barely high enough to retain material from even the slowest reported winds of IM-AGB stars (i.e.,  $\sim 10 \text{ km s}^{-1}$ ). However, the escape velocities were significantly higher at an age of  $10^7$  yr, as illustrated by the right panel of Figure 4. Moreover, the clusters with  $v_{esc,7} \gtrsim 15 \text{ km s}^{-1}$  have significantly higher values of  $C_{rel}$  than those with  $v_{esc,7} \lesssim 10 \text{ km s}^{-1}$ , and the correlation between  $C_{rel}$  and  $v_{esc}$  becomes stronger than in the left panel. These trends are present whether or not one takes initial mass segregation of stars into account in the calculations of  $v_{esc,7}$ . Summarizing these results, it appears that intermediate-age star clusters in the LMC with higher (initial) escape velocities have upper (“younger”) MSTO stars that are more centrally concentrated than their counterparts in the lower (“older”) MSTO. This finding is discussed further in Section 4 below. The one cluster that seems to deviate slightly from the trends mentioned above and shown in Figure 4 is NGC 1783. This is the cluster with the largest radius among our sample. In fact, its radial extent is so large that the field of view of the *HST*/ACS image is too small to allow a robust determination of its King concentration parameter (see Paper II), which translates into a relatively large uncertainty in its half-light radius and hence in its escape velocity. Future determinations of its  $r_h$  from wider-field imaging should help improve the accuracy of its escape velocity and hence its position in Figure 4.

#### 4. IMPLICATIONS REGARDING THE NATURE OF MULTIPLE POPULATIONS IN STAR CLUSTERS

The results described above have implications regarding the nature of multiple stellar generations in star clusters in general, including the situation seen in many (ancient) GCs in our

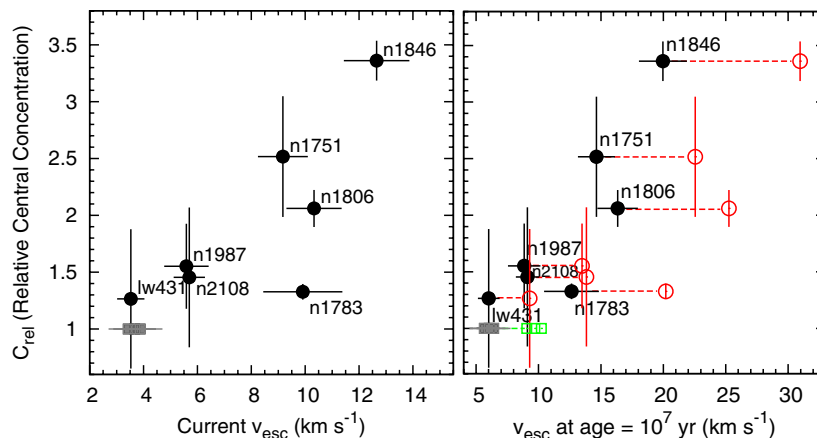


**Figure 4.** Left panel: parameter  $C_{rel}$ , a measure of the relative central concentration of the upper vs. the lower half of the MSTO region (cf. Equation. (4)), plotted against *current* escape velocity. Right panel:  $C_{rel}$  against escape velocity at an age of  $10^7$  yr. Filled circles represent data for clusters in our sample using a model without initial mass segregation while open (red) circles do so using a model involving initial mass segregation. Clusters shown by Milone et al. (2009) not to exhibit eMSTO regions are represented by filled (gray) squares and open (green) squares for models without and with initial mass segregation, respectively. The names of the star clusters in our sample are indicated to the upper or lower right of their data points. See discussion in Section 3.3.

(A color version of this figure is available in the online journal.)

Galaxy. To constrain the scope of this broad topic somewhat, we restrict the following discussion to the case of star clusters that were never massive enough to retain gas expelled by energetic SN explosions and/or to capture significant numbers of field stars (e.g., from their host dwarf galaxies). In practice, this restriction corresponds roughly to the exclusion of ancient star clusters with current masses  $\gtrsim 2 \times 10^6 M_\odot$  (cf. Bastian & Goodwin 2006; Fellhauer et al. 2006) at an age of 13 Gyr. The LMC star clusters studied in this paper are and were indeed always less massive than that limit.

Star clusters in our sample with initial escape velocities  $v_{\text{esc},7} > 15 \text{ km s}^{-1}$  have  $C_{\text{rel}}$  values that are significantly higher than unity and correlate with  $v_{\text{esc},7}$ . Hence we postulate that the extended morphology of their MSTO is caused mainly by a range in age, although we cannot formally rule out that the widening of the MSTO is partly due to an additional physical process for those clusters as well.

As to the star clusters in our sample with initial escape velocities  $v_{\text{esc},7} \lesssim 10 \text{ km s}^{-1}$ , they have  $C_{\text{rel}}$  values consistent with unity. Under the assumption that the material used to form secondary generations of stars within clusters is mainly produced internally from stellar winds with  $v \gtrsim 10\text{--}15 \text{ km s}^{-1}$ , it seems plausible that eMSTO regions in such clusters may be due in part to physical processes unrelated to a range in age, e.g., one or more processes that are independent of (or only slightly dependent on) the location of stars within the cluster. This could be a range of stellar rotation velocities as proposed by Bastian & de Mink (2009) and/or other (yet unidentified) physical processes, possibly related to interactions between close binary stars since the binary fractions are significant (15%–35%, cf. Paper II) in the clusters studied here. Note, however, that the fact that the clusters found by Milone et al. (2009) *not* to harbor eMSTOs are all at the low end of the mass (and  $v_{\text{esc},7}$ ) range of the clusters considered here seems inconsistent with the stellar rotation scenario in that one would not a priori expect the distribution of stellar rotation rates to depend on cluster mass or escape velocity. In this context we note that an age range would still be able to account for a widening of the MSTO in low-mass clusters in our sample in case their escape velocities at an age of  $10^7 \text{ yr}$  turn out to be higher than our estimates. This would, for example, be the case if the initial mass segregation of such clusters was stronger than in the model we used in Section 3.3.2. In that case, the low values of  $C_{\text{rel}}$  in these low-mass clusters can still be explained by their short half-mass relaxation times which are significantly shorter than their age (cf. Table 2) so that initial differences in radial distribution between generations of stars would now have been eliminated.

These results impact our understanding of multiple populations in ancient GCs. For example, the finding of multiple populations and an Na–O anticorrelation in M 4 (Marino et al. 2008, and references therein) was described as surprising given its low mass of  $\sim 6 \times 10^4 M_\odot$ . However, using its current values for half-light radius  $r_h = 2.23 \text{ pc}$  and King concentration parameter  $c = 39$  (Harris 1996), an age of 13 Gyr, and the methodology outlined in Section 3.3, we calculate a present-day escape velocity  $v_{\text{esc}} = 16 \text{ km s}^{-1}$  and a  $v_{\text{esc},7} = 52 \text{ km s}^{-1}$  for M 4 (assuming no initial mass segregation). This is more than sufficient to have retained chemically enriched material from slow stellar winds of the first stellar generation. In fact, for typical half-mass cluster radii  $r_h \lesssim 3 \text{ pc}$ , we would expect ancient star clusters with current masses as low as  $\sim 5 \times 10^3 M_\odot$  to have been able to retain such material (see also Conroy 2011 for a scenario based on evolution of cluster masses).

Similarly, recent results on the presence or the absence of significant light element abundance variations within LMC clusters can be understood by considering the clusters’ initial escape velocities. Mucciarelli et al. (2009) measured Na and O abundances for RGB stars in three old metal-poor GCs in the LMC which have current masses in the range  $2\text{--}4 \times 10^5 M_\odot$  (see Mackey & Gilmore 2003), and found clear evidence for Na–O anticorrelations similar to those observed in Galactic GCs. On the other hand, Mucciarelli et al. (2008) measured element abundances in four relatively massive intermediate-age (1–2 Gyr) clusters in the LMC and found only small variations of element abundance ratios within each cluster. However, focusing on their [Na/Fe] measurements, we note that two clusters in their sample (NGC 1978 and NGC 2173) exhibit a range of [Na/Fe] values  $\Delta[\text{Na/Fe}] \geq 0.4 \text{ dex}$  which is a  $\geq 4\sigma$  effect where  $\sigma$  is the typical measurement error of [Na/Fe].<sup>5</sup> More recently, Mucciarelli et al. (2011) measured element abundances of 14 stars in the young GC NGC 1866 in the LMC and found no sign of an Na–O anticorrelation (nor a significant spread in [Na/Fe]). Since they also did not detect Na–O anticorrelations in the massive intermediate-age clusters in their 2008 paper, they argued for “a different formation/evolution scenario for the LMC massive clusters younger than  $\sim 3 \text{ Gyr}$  with respect to the old ones.” To evaluate whether the presence or the absence of significant spreads in [Na/Fe] in the LMC clusters studied by Mucciarelli et al. (2008, 2009, 2011) could instead “simply” be due to the clusters’ masses and escape velocities at an age of 10 Myr, we first adopt these clusters’ current masses, radii, and ages from the compilation of Mackey & Gilmore (2003). Since NGC 1978 was not included in that compilation, we adopt its age, [Fe/H] and  $E(B - V)$  from Milone et al. (2009), we assume a radius of  $r_h = 8 \pm 4 \text{ pc}$  (cf. Section 3.3), and we estimate its current mass from its integrated  $V$  magnitude in Goudfrooij et al. (2006) and the  $\mathcal{M}/L_V$  ratios of the Bruzual & Charlot (2003) SSP models using the Chabrier IMF. We then estimate these clusters’ masses and escape velocities at an age of 10 Myr using the methodology described in Section 3.3. We plot the observed spreads in [Na/Fe] (defined here as  $\Delta([\text{Na/Fe}])$ ) from Mucciarelli et al. (2008, 2009, 2011) as well as the current cluster masses versus  $v_{\text{esc},7}$  in Figure 5. Note that (1) the distinction between clusters with and without significant ( $\sim 4\sigma$ ) spreads in [Na/Fe] is found at  $v_{\text{esc},7} \approx 15 \text{ km s}^{-1}$  at an age of 10 Myr, and (2)  $\Delta([\text{Na/Fe}])$  correlates with  $v_{\text{esc},7}$ , indicating that clusters with higher initial escape velocities are able to retain material with higher variance of light element abundances. This is consistent with the results shown in Figure 4 for the  $C_{\text{rel}}$  parameter of the clusters in our sample and underlines the importance of the clusters’ initial escape velocities in their ability to retain slow wind material from stars of the first generation.

Our results for the star clusters with  $v_{\text{esc},7} \gtrsim 15 \text{ km s}^{-1}$  are generally consistent with the conclusions drawn for NGC 1846 in Paper I (see also Renzini 2008; Conroy & Spergel 2011). In particular, we believe our results are most consistent with the “in situ” scenario (e.g., D’Ercole et al. 2008; Renzini 2008) in which star clusters with masses high enough to retain ejecta in slow winds of stars of the first generation gather this material in their central regions where second-generation star formation

<sup>5</sup> The negligible variation of [O/Fe] in these clusters found by Mucciarelli et al. (2008) can be explained by their moderately high metallicities for which depletion of O in IM–AGB stars is much smaller than for the much more metal-poor ancient GCs in the LMC (Ventura & D’Antona 2009; Conroy 2011).

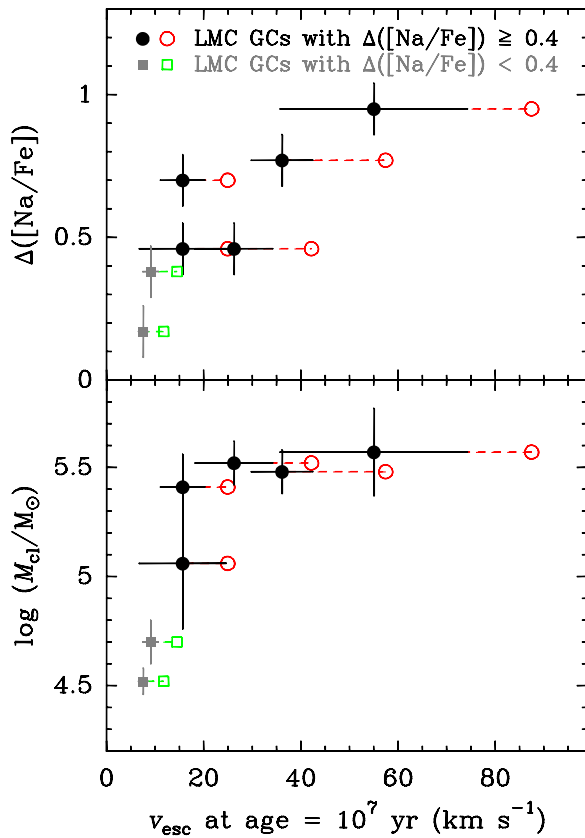


**Figure 5.** Top panel:  $\Delta([\text{Na}/\text{Fe}])$ , defined as the measured spread in  $[\text{Na}/\text{Fe}]$  among stars in LMC clusters studied by Mucciarelli et al. (2008, 2009, 2011), vs. cluster escape velocity at an age of 10 Myr. Error bars for  $\Delta([\text{Na}/\text{Fe}])$  indicate the typical uncertainty of individual  $[\text{Na}/\text{Fe}]$  measurements. Bottom panel: present-day cluster mass against escape velocity at an age of  $10^7$  yr for the same clusters. Filled (black) circles represent data for clusters with  $\Delta([\text{Na}/\text{Fe}]) \geq 0.4$  (a  $4\sigma$  effect) using a model without initial mass segregation, while open (red) circles do so using a model involving initial mass segregation. Clusters with  $\Delta([\text{Na}/\text{Fe}]) < 0.4$  are represented by filled (gray) squares and open (green) squares for models without and with initial mass segregation, respectively. See discussion in Section 4.

(A color version of this figure is available in the online journal.)

can occur. The observed relation between the parameter  $C_{\text{rel}}$  and the initial escape velocity of the cluster strongly suggests that this is taking place. In the context of this scenario, we recall that the hitherto suggested source(s) of the ejecta are FRMS (Decressin et al. 2007), massive binary stars (de Mink et al. 2009), and IM-AGB stars (e.g., D’Antona & Ventura 2007). Note that the ejecta from FRMS and massive binary stars are produced on timescales that are significantly shorter than those from IM-AGB stars ( $\sim 10\text{--}30$  Myr versus  $\sim 50\text{--}300$  Myr, respectively; see, e.g., Decressin et al. 2007; Ventura & D’Antona 2008). That is, all material created by massive stars that could be used to form second-generation stars would be available in the cluster by the time IM-AGB stars would *start* their slow mass loss. To compare these timescales to the age distributions of the eMSTO clusters in our sample, we show the latter in Figure 6, reproduced from Papers I and II. Note that Monte Carlo simulations described in Paper II show that two populations with ages separated by 100–150 Myr or more would result in observable bimodality in our age distributions derived from the MSTO photometry. Hence, the combination of the observed age ranges of 200–500 Myr, the fact that the material lost from first-generation stars throughout the cluster needs some time to

accumulate in the central regions to allow second-generation star formation to occur, and the absence of clear bimodality in the age distributions seems to suggest at face value that FRMS and/or massive binary stars could well be significant contributors to the enriched material used to produce the second stellar generation. However, IM-AGB stars also seem likely significant contributors, since the age distributions of the star clusters with the highest escape velocities in our sample do typically peak near the younger end of the observed age range (especially for the more massive clusters in our sample).

Our results also have an impact on an argument made against the “in situ” scenario that if indeed the eMSTO phenomenon reflects a range of ages and the second generation of stars is formed from material produced by first-generation stars, why are no eMSTOs seen in clusters with ages similar to the typical spread in ages within eMSTO clusters (i.e., 100–500 Myr)? The answer seems to be, at least in part, that the escape velocities of clusters in this age range that are nearby enough to detect the presence of an eMSTO are not high enough to retain the ejecta of the first-generation stars. Using the masses and radii derived by the study of Mackey & Gilmore (2003) for Magellanic Cloud clusters in that age range and applying our methodology described in Section 3.3, we find that there is only one such cluster (NGC 1856,  $\log M_{\text{cl}}/M_{\odot} \sim 4.9$ ,  $r_{\text{h}} \sim 3.2$  pc,  $\log \text{Age} = 8.12$ ) that has a  $v_{\text{esc},7}$  value above  $15 \text{ km s}^{-1}$ , i.e., sufficient to retain gas lost by slow stellar winds of the first generation. Unfortunately, the currently available photometric data for this cluster are inadequate to properly assess the presence of a range of ages. Keller et al. (2011) also recently made an additional, statistically based argument suggesting that the absence of eMSTO clusters in the age range of 100–300 Myr is not problematic to the “in situ” scenario.

In addition to the “in situ” scenario, part of the gas used to form second-generation stars may have been accreted from the ambient ISM  $\gtrsim 10^8$  yr after the first generation was formed (see Conroy & Spergel 2011; Pflamm-Altenburg & Kroupa 2009). This scenario is attractive in that (1) it addresses the concern that the high fraction of second-generation stars in GCs seems to require more gas than any suggested type of donor stars can provide and (2) gas from the ambient ISM readily provides the “dilution” that is likely needed to create the smooth Na–O anticorrelations seen in ancient Galactic GCs (e.g., Ventura & D’Antona 2008, 2009). In the absence of such dilution, one would expect a more discrete distribution of cluster stars in the  $[\text{Na}/\text{Fe}]$  versus  $[\text{O}/\text{Fe}]$  diagram than that observed (see, e.g., Carretta et al. 2009). However, the uniformity of massive element abundances (e.g.,  $[\text{Fe}/\text{H}]$  and  $[\text{Ca}/\text{H}]$ ) among stars in Galactic GCs (except for the most massive ones such as  $\omega$  Cen and M 54) and the razor-sharp RGB sequences seen in the CMDs of the more massive LMC star clusters in our sample (cf. Paper II) do require that the spread in  $[\text{Fe}/\text{H}]$  and  $[\text{Ca}/\text{H}]$  in the ambient ISM was very small when the second-generation stars were formed. Future measurements of  $[\text{Fe}/\text{H}]$  and  $[\text{Ca}/\text{H}]$  variations among RGB stars in the LMC field population may be able to address this concern. A next generation of theoretical simulations similar to those used by D’Ercole et al. (2008, 2010) may well be able to shed more light on the expected relative contributions of the possible donor star types after taking into account their respective numbers of stars from the IMF (see, e.g., de Mink et al. 2009), their typical evolutionary timescales, the abundance patterns of their ejecta, and the mass evolution of star clusters containing multiple generations of stars.

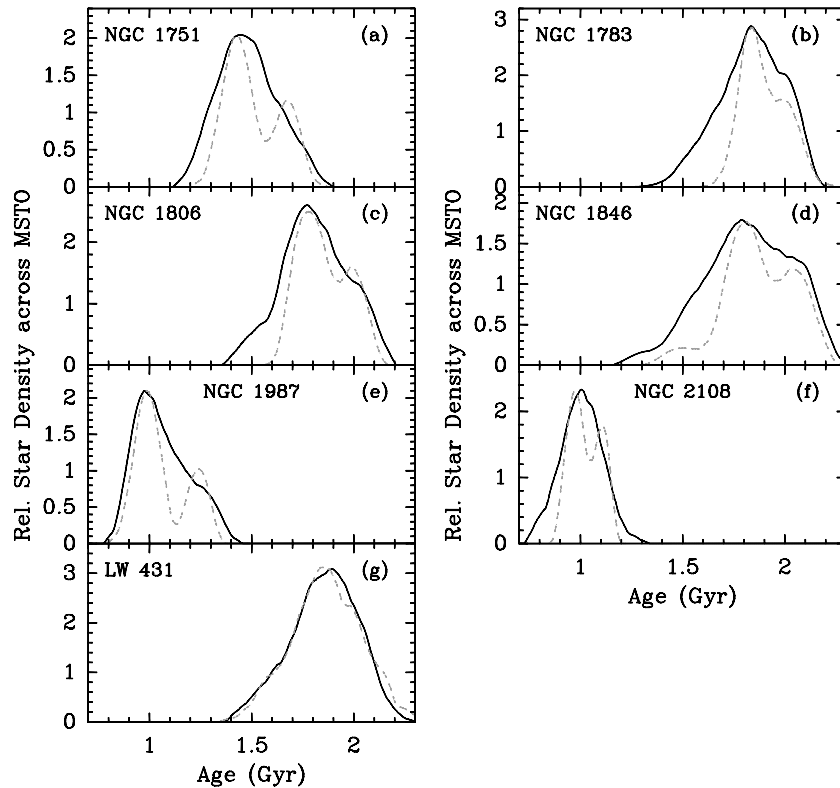


**Figure 6.** Age distributions of the clusters in our sample, reproduced from Papers I and II, derived from probability density profiles of the number density of stars across the eMSTO regions. The solid lines represent cluster stars. For comparison, the gray dashed lines represent the best-fit two-SSP simulations of the clusters’ age distributions. See Paper II for details. The names of the star clusters are indicated in the legend of each panel. See discussion in Section 4.

## 5. SUMMARY AND CONCLUSIONS

We analyzed dynamical properties of 11 intermediate-age star clusters in the LMC that have high-precision ages and metallicities measured from recent *HST*/ACS photometry. Seven of these 11 clusters contain MSTO regions that are significantly more extended than expected from measurement errors.

For the three massive clusters NGC 1751, NGC 1806, and NGC 1846, we find that radial distributions of stars in the upper (i.e., brighter) half of the eMSTO region are significantly more centrally concentrated than stars in the lower (i.e., fainter) half of the eMSTO region as well as the (more massive) RGB and AGB. Since this cannot be due to dynamical evolution of an SSP, we conclude that the upper and lower MSTO regions in those clusters correspond to intrinsically different populations which have undergone different amounts of violent relaxation during their collapse. To look for an explanation for this finding, we calculate the evolution of mass and escape velocity for the clusters in our sample from an age of  $10^7$  yr to the present time, using a combination of stellar evolution models and dynamical cluster disruption models. The three star clusters mentioned above turn out to be the only three clusters in our sample that have the following two properties: (1) escape velocities  $v_{\text{esc}} \gtrsim 15 \text{ km s}^{-1}$  at an age of  $10^7$  yr, i.e., large enough to retain material shed by slow stellar winds of the first generation, and (2) half-mass relaxation times that are larger than or equal to their age. At least for these clusters, we suggest that the main cause of the presence of the eMSTO region is a range of stellar ages within the cluster. The data seem most consistent with the “in situ” scenario in which secondary generations of stars form within the cluster itself out of gas ejected by stars of the first stellar generation that feature slow stellar winds.

Viable sources of the enriched material are thought to include FRMS, massive binary stars, and intermediate-mass AGB stars. Element abundance ratios from high-resolution spectroscopy of individual cluster stars should be very useful in further constraining the nature of the eMSTO regions in massive intermediate-age star clusters. In particular, one would expect to see correlated variations in light element abundances (e.g., N, O, Na) among the stars in the star clusters with relatively high escape velocities in our sample, likely in a way similar to the Na–O anticorrelation found in ancient GCs.

We acknowledge stimulating discussions with Aaron Dotter, Iskren Georgiev, Leo Girardi, Selma de Mink, and Enrico Vesperini. We gratefully acknowledge the thoughtful comments and suggestions of the anonymous referee. T.H.P. acknowledges support by the FONDAP Center for Astrophysics 15010003 and BASAL Center for Astrophysics and Associated Technologies PFB-06, Conicyt, Chile. R.C. acknowledges support from the National Science Foundation through CAREER award 0847467. This research was supported in part by the National Science Foundation under Grant No. PHY05-51164. Support for *HST* Program GO-10595 was provided by NASA through a grant from the Space Telescope Science Institute, which is operated by the Association of Universities for Research in Astronomy, Inc., under NASA contract NAS5-26555.

## REFERENCES

- Anderson, J., Piotto, G., King, I. R., Bedin, L. R., & Guthathakurta, P. 2009, *ApJ*, **697**, L58  
 Bastian, N., & de Mink, S. E. 2009, *MNRAS*, **398**, L11  
 Bastian, N., & Goodwin, S. P. 2006, *MNRAS*, **369**, L9

- Baumgardt, H., & Kroupa, P. 2007, *MNRAS*, **380**, 1589
- Baumgardt, H., Kroupa, P., & Parmentier, G. 2008, *MNRAS*, **384**, 1231
- Bellini, A., Piotto, G., Bedin, L. R., King, I. R., Anderson, J., Milone, A. P., & Momany, Y. 2009, *A&A*, **507**, 1393
- Bica, E., Clariá, J. J., Dottori, H., Santos, J. F. C., & Piatti, A. E. 1996, *ApJS*, **102**, 57
- Binney, J., & Tremaine, S. 1987, *Galactic Dynamics* (Princeton Series in Astrophysics; Princeton, NJ: Princeton Univ. Press), 337
- Bruzual, G. A., & Charlot, S. 2003, *MNRAS*, **344**, 1000
- Carretta, E., et al. 2009, *A&A*, **505**, 117
- Carretta, E., et al. 2010, *ApJ*, **714**, L7
- Chabrier, G. 2003, *PASP*, **115**, 763
- Chernoff, D. F., & Weinberg, M. D. 1990, *ApJ*, **351**, 121
- Conroy, C. 2011, *ApJ*, submitted (arXiv:1101.2208v1)
- Conroy, C., & Spergel, D. N. 2011, *ApJ*, **726**, 36
- D'Antona, F., & Ventura, P. 2007, *MNRAS*, **379**, 1431
- Decressin, T., Meynet, G., Charbonnel, C., Prantzos, N., & Ekström, S. 2007, *A&A*, **464**, 1029
- de Mink, S. E., Pols, O. R., Langer, N., & Izzard, R. G. 2009, *A&A*, **5007**, L1
- D'Ercole, A., D'Antona, F., Ventura, P., Vesperini, E., & McMillan, S. L. W. 2010, *MNRAS*, **407**, 854
- D'Ercole, A., Vesperini, E., D'Antona, F., McMillan, S. L. W., & Recchi, S. 2008, *MNRAS*, **391**, 825
- Fall, S. M., & Zhang, Q. 2001, *ApJ*, **561**, 751
- Fellhauer, M., Kroupa, P., & Evans, N. W. 2006, *MNRAS*, **372**, 338
- Fukushige, T., & Heggie, D. C. 1995, *MNRAS*, **276**, 206
- Georgiev, I. Y., Hilker, M., Puzia, T. H., Goudfrooij, P., & Baumgardt, H. 2009, *MNRAS*, **396**, 1075
- Girardi, L., Eggenberger, P., & Miglio, A. 2011, *MNRAS*, **412**, L103
- Girardi, L., Rubele, S., & Kerber, L. 2009, *MNRAS*, **394**, L74
- Glatt, K., et al. 2008, *AJ*, **135**, 1703
- Goudfrooij, P., Gilmore, D., Kissler-Patig, M., & Maraston, C. 2006, *MNRAS*, **369**, 697
- Goudfrooij, P., Puzia, T. H., Kozhurina-Platais, V., & Chandar, R. 2009, *AJ*, **137**, 4988 (Paper I)
- Goudfrooij, P., Puzia, T. H., Kozhurina-Platais, V., & Chandar, R. 2011, *ApJ*, **737**, 3 (Paper II)
- Gratton, R., Sneden, C., & Carretta, E. 2004, *ARA&A*, **42**, 385
- Harris, W. E. 1996, *ApJ*, **112**, 1487
- Hilker, M., & Richtler, T. 2000, *A&A*, **362**, 895
- Hills, J. G. 1980, *ApJ*, **235**, 986
- Keller, S. C. 2004, *PASA*, **21**, 310
- Keller, S. C., Mackey, A. D., & Da Costa, G. S. 2011, *ApJ*, **731**, 22
- King, I. 1962, *AJ*, **67**, 471
- Lee, Y., Joo, J., Sohn, Y., Rey, S., Lee, H., & Walker, A. R. 1999, *Nature*, **402**, 55
- Mackey, A. D., Broby Nielsen, P., Ferguson, A. M. N., & Richardson, J. C. 2008, *ApJ*, **681**, L17
- Mackey, A. D., & Gilmore, G. F. 2003, *MNRAS*, **338**, 85
- Marino, A. F., Villanova, S., Piotto, G., Milone, A. P., Momany, Y., Bedin, L. R., & Medling, A. M. 2008, *A&A*, **490**, 625
- Marshall, J. R., van Loon, J. T., Matsuura, M., Wood, P. R., Zijlstra, A. A., & Whitelock, P. A. 2004, *MNRAS*, **355**, 1348
- McLaughlin, D. E., & Fall, S. M. 2008, *ApJ*, **679**, 1272
- Meylan, G., & Heggie, D. C. 1997, *A&AR*, **8**, 1
- Milone, A. P., Bedin, L. R., Piotto, G., & Anderson, J. 2009, *A&A*, **497**, 755
- Milone, A. P., et al. 2008, *ApJ*, **673**, 241
- Mucciarelli, A., Carretta, E., Origlia, L., & Ferraro, F. R. 2008, *AJ*, **136**, 375
- Mucciarelli, A., Origlia, L., Ferraro, F. R., & Pancino, E. 2009, *ApJ*, **695**, L134
- Mucciarelli, A., et al. 2011, *MNRAS*, **413**, 837
- Pflamm-Altenburg, J., & Kroupa, P. 2009, *MNRAS*, **397**, 488
- Piotto, G., et al. 2007, *ApJ*, **661**, L53
- Porter, J. M. 1996, *MNRAS*, **280**, L31
- Porter, J. M., & Rivinius, T. 2003, *PASP*, **115**, 1153
- Renzini, A. 2008, *MNRAS*, **391**, 354
- Rubele, S., Girardi, L., Kozhurina-Platais, V., Goudfrooij, P., & Kerber, L. 2011, *MNRAS*, **414**, 2204
- Rubele, S., Kerber, L., & Girardi, L. 2010, *MNRAS*, **403**, 1156
- Salpeter, E. E. 1955, *ApJ*, **121**, 161
- Sarajedini, A., & Layden, A. C. 1995, *AJ*, **109**, 1086
- Saslaw, W. C. 1985, *Gravitational Physics of Stellar and Galactic Systems* (Cambridge: Cambridge Univ. Press)
- Searle, L., Wilkinson, A., & Bagnuolo, W. G. 1980, *ApJ*, **239**, 803
- Smith, N., Gehrz, R. D., Stahl, O., Balick, B., & Kaufer, A. 2002, *ApJ*, **578**, 464
- Spitzer, L., Jr. 1987, *Dynamical Evolution of Globular Clusters* (Princeton, NJ: Princeton Univ. Press)
- Strom, S. E., Wolff, S. C., & Dror, D. H. A. 2005, *AJ*, **129**, 809
- Vassiliadis, E., & Wood, P. R. 1993, *ApJ*, **413**, 641
- Ventura, P., & D'Antona, F. 2008, *MNRAS*, **385**, 2034
- Ventura, P., & D'Antona, F. 2009, *A&A*, **499**, 835
- Vesperini, E., McMillan, S. L. W., & Portegies Zwart, S. 2009, *ApJ*, **698**, 615
- Villanova, S., et al. 2008, *ApJ*, **663**, 296
- Weidner, C., & Kroupa, P. 2006, *MNRAS*, **365**, 1333
- Wünsch, R., Tenorio-Tagle, G., & Palouš Silich, S. 2008, *ApJ*, **683**, 683